Earth and Planetary Science Letters 562 (2021) 116845

Contents lists available at ScienceDirect

Earth and Planetary Science Letters

www.elsevier.com/locate/epsl

Preconditioning by sediment accumulation can produce powerful turbidity currents without major external triggers

Lewis P. Bailey [a,b,*], Michael A. Clare [a], Kurt J. Rosenberger [c], Matthieu J.B. Cartigny [d], Peter J. Talling [d], Charles K. Paull [e], Roberto Gwiazda [e], Daniel R. Parsons [f], Stephen M. Simmons [f], Jingping Xu [g], Ivan D. Haigh [b], Katherine L. Maier [c,e,h], Mary McGann [i], Eve Lundsten [e] and the Monterey CCE Team

[a] National Oceanography Centre, Southampton, SO14 3ZH, UK
[b] School of Ocean and Earth Science, University of Southampton, Southampton, SO14 3ZH, UK
[c] Pacific Coastal and Marine Science Center, U.S. Geological Survey, Santa Cruz, CA 95060, USA
[d] Departments of Geography and Earth Science, Durham University, Durham, DH1 3LE, UK
[e] Monterey Bay Aquarium Research Institute, Moss Landing, CA 95039, USA
[f] Energy and Environment Institute, University of Hull, Hull, HU6 7RX, UK
[g] Southern University of Science and Technology, 518055 Shenzhen, China
[h] National Institute of Water and Atmospheric Research, Wellington 6241, New Zealand
[i] Pacific Coastal and Marine Science Center, U.S. Geological Survey, Menlo Park, CA 94025, USA

ARTICLE INFO

Article history:
Received 19 May 2020
Received in revised form 9 February 2021
Accepted 17 February 2021
Available online 3 March 2021
Editor: J.-P. Avouac

Dataset link:
https://www.mbari.org/science/seafloor-processes/geological-changes/coordinated-canyon-experiment-datareport-main-page/

Dataset link:
https://www.sciencebase.gov/catalog/item/5a74c1fce4b00f54eb1c828f

Keywords:
submarine canyon
turbidity current
geohazard
direct monitoring
preconditioning
triggering

ABSTRACT

Turbidity currents dominate sediment transfer into the deep ocean, and can damage critical seabed infrastructure. It is commonly inferred that powerful turbidity currents are triggered by major external events, such as storms, river floods, or earthquakes. However, basic models for turbidity current triggering remain poorly tested, with few studies accurately recording precise flow timing. Here, we analyse the most detailed series of measurements yet made of powerful (up to 7.2 $m\,s^{-1}$) turbidity currents, within Monterey Canyon, offshore California. During 18-months of instrument deployment, fourteen turbidity currents were directly monitored. No consistent triggering mechanism was observed, though flows did cluster around enhanced seasonal sediment supply. We compare turbidity current timing at Monterey Canyon (a sandy canyon-head fed by longshore drift) to the only other systems where numerous (>10-100) flows have been measured precisely via direct monitoring; the Squamish Delta (a sandy fjord-head delta), and the Congo Canyon (connected to the mud-dominated mouth of the Congo River). A common seasonal pattern emerges, leading to a new model for preconditioning and triggering of turbidity currents initiating through slope failure in areas of sediment accumulation, such as canyon heads or river mouths. In this model, rapid or sustained sediment supply alone can produce elevated pore pressures, which may persist, thereby predisposing slopes to fail. Once preconditioned, a range of minor external perturbations, such as moderate storm-waves, result in local pore pressure variation, and thus become effective triggers. Major external triggers are therefore not always a prerequisite for triggering of powerful turbidity currents.

1. Introduction

Turbidity currents are one of the most important processes for moving sediment across our planet, dominating transport from continental shelves to the deep sea, and play a key role in the transport and burial of organic carbon (Galy et al., 2007) and pollutants (Mordecai et al., 2011). These submarine flows can reach velocities of up to 20 $m\,s^{-1}$ (Hsu et al., 2008) and runout for hundreds of kilometres (Piper et al., 1999). Powerful turbidity currents can break important seafloor infrastructure, such as telecommunication cables that today carry over 95% of transoceanic data traffic (e.g. Heezen and Ewing, 1952; Heezen et al., 1964; Piper et al., 1999; Hsu et al., 2008; Carter et al., 2009, 2012; Gavey et al., 2017; Pope et al., 2017).

Given their role in global sediment transport, and their potential for damaging critical infrastructure, it is important to un-

* Corresponding author at: National Oceanography Centre, Southampton, SO14 3ZH, UK.
E-mail address: l.bailey@soton.ac.uk (L.P. Bailey).

https://doi.org/10.1016/j.epsl.2021.116845

Table 1
Summary of previous studies of how turbidity currents are triggered in submarine canyons and channels with different types of sediment supply, based on precise timings of flow events measured via direct monitoring.

Sediment supply	Site	Flows	Period	Triggers	Reference
River-fed fjords	Knight Inlet, Canada Bute Inlet, Canada	39 35	17 months 13 months	Elevation in freshet river discharge.	Bornhold et al., 1994
	Squamish Prodelta, Canada	106	147 days	System active during river discharge >300 m^3/s. Tidal drawdown or rapid sedimentation trigger.	Clare et al., 2016; Hizzett et al., 2018
River-fed canyons	Congo Canyon, offshore Angola	6	4 months	Elevated river discharge but not flood peaks.	Heezen et al., 1964; Azpiroz-Zabala et al., 2017
	Gaoping Canyon, offshore Taiwan	23	3.5 years	Flow initiates following typhoon elevation of river discharge.	Zhang et al., 2018
		2	2 months	Typhoon-triggered hyperpycnal flows.	Liu et al., 2012
		Cable Breaks		River flooding, tropical cyclones and earthquakes.	Hsu et al., 2008; Carter et al., 2012; Pope et al., 2017
	Gulf of Lions canyon system, Mediterranean	6	4 months	Dense shelf water cascading, storms, river flooding and trawling.	Canals et al., 2006
	Var Canyon, Mediterranean	8	2 years	Hyperpycnal flows during river flooding and some local storms.	Khripounoff et al., 2009
Littoral drift-fed canyons	Eel River Shelf and Canyon, offshore California	11	83 days	Storms, not directly linked to river floods.	Puig et al., 2004
	Hueneme & Mugu Canyons, offshore California	6	6 months	Storms. The same storm event is capable of triggering flows in both canyons simultaneously.	Xu et al., 2010
	Monterey Canyon, offshore California	4 10	11 months 16 & 26 months	Coincident with elevation in storm activity.	Xu et al., 2004 Paull et al., 2003, 2010
	Nazare Canyon, offshore Portugal	3	22 months	Storm waves with potential contribution from flooding north of the canyon head.	Martín et al., 2011
Sediment starved canyon	Gulf of St. Lawrence, East Canada	4	27 months	Sustained storms resuspend sediment in canyon heads.	Normandeau et al., 2020

derstand what controls turbidity current activity. Previous studies commonly infer that turbidity currents are caused by major external events, such as storms, river floods or major earthquakes (Table 1). Turbidity current deposits ('turbidites') may then provide valuable records of such events that can be extended beyond historical or instrumental archives (e.g. Mulder et al., 2001; Goldfinger, 2011). To interpret the turbidite record, it is thus important to understand whether turbidity currents can sometimes be triggered without a major external trigger, and whether the nature or magnitude of the trigger can be linked to flow velocity or runout distance.

This contribution seeks to understand the roles of preconditioning and triggering factors and how these control turbidity current activity, timing and frequency. Previous work demonstrates multiple mechanisms are capable of generating turbidity currents (Table 1; Talling, 2014). Mechanisms of initiation vary across different settings. For example, where submarine canyons have direct fluvial input, plunging of (hyperpycnal) river floodwater can produce turbidity currents, if the floodwater contains sufficient sediment to be denser than seawater (label 1 in Fig. 1; Mulder and Syvitski, 1995; Johnson et al., 2001; Khripounoff et al., 2009). Rivers with lower sediment concentrations generate surface (homopycnal) plumes. Sediment settling from surface plumes can also generate turbidity currents, including via sediment trapping due to convergent near-bed flow, and episodic remobilisation on the bed (label 2 in Fig. 1; Hage et al., 2019). Flows can also form via disintegration of submarine slope failures (label 3; Piper et al., 1999). Initiation through slope failure is typically a result of preconditioning factors, especially development of high excess pore pressures (e.g. Masson et al., 2010; Dugan and Sheahan, 2012; Talling et al., 2014). Such excess pore pressures are favoured in locations where sedimentation is rapid, and pore fluid can be trapped by less permeable layers (Özener et al., 2009). Short period events that instantaneously initiate the flow are referred to as triggers. These include earthquake shaking (label 4; Piper et al., 1999; Mountjoy et al., 2018), low tides unloading seabed sediment (label 5; Hughes Clarke et al., 2014; Clare et al., 2016), and cyclic loading as a result of storm waves or surges (label 6; Chamberlain, 1964; Puig et al., 2004). Sediment may also be resuspended as shelf sediment plumes during storms (label 7; Inman et al., 1976; Normandeau et al., 2020), following trawling (Puig et al., 2012) or due to cascading of dense water (label 8; Canals et al., 2006; Puig et al., 2013). Internal tides (label 9) may also cause resuspension of sediment, triggering dilute flows (label 10; Martín et al., 2011).

Testing models for how turbidity currents are triggered requires measuring the timing of turbidity currents and potential triggers with precision. For example, over days to hours, a storm may generate both large wave heights (causing cyclic loading of the seafloor) at its peak, and river flooding (initiating a plunging hyperpycnal flow) following its passage (Pope et al., 2017). The precise start time of a turbidity current is needed to distinguish between these different triggers. Only in rare cases (e.g. Ikehara et al., 2014) can deposits be dated at sufficiently high resolution to directly isolate such external triggers, therefore more robust constraints on flow timing are needed. Precise timing can be provided by seafloor cable breaks or direct monitoring of turbidity currents; however, cable breaks fail to measure weaker events that leave cables intact, and breakages may not occur at the timing of flow impact. The accuracy of instruments used in direct flow monitoring, such as Acoustic Doppler current profilers (ADCPs), is a function of data resolution and distance from source. Previous studies using ADCPs have either collected data at low temporal resolution, or involved instruments located far away from where flows originate. Moreover, monitoring instruments were typically deployed for a few months, missing parts of annual or longer cycles. This ensures that the controls on turbidity currents activity remain poorly tested (Table 1).

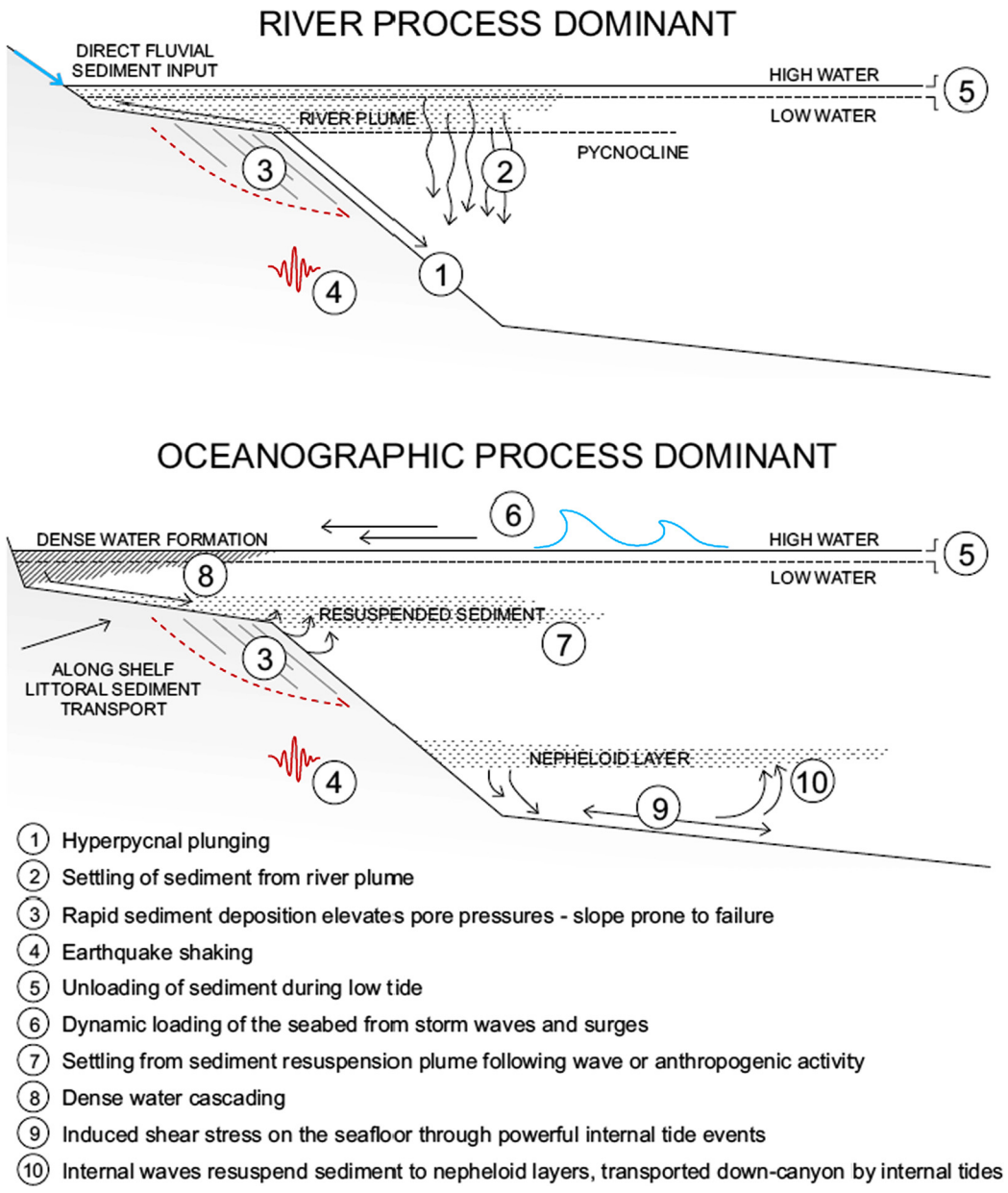

Fig. 1. Previous hypotheses for initiation, preconditioning and triggering mechanisms of turbidity currents in submarine canyons.

Here, we analyse the most detailed measurements yet of oceanic turbidity currents (Paull et al., 2018). Data were collected during the 18-month-long Coordinated Canyon Experiment (CCE) in Monterey Canyon, offshore California (Fig. 2). No previous direct monitoring has deployed such a dense network of novel equipment to record high-resolution measurements of turbidity currents at multiple locations along their path. The longevity of the monitoring period also allows investigation of seasonal patterns in turbidity current activity. Our aim is to understand the roles of preconditioning and triggering mechanisms on the timing of turbidity currents. We address the following specific aims. First, using the uniquely detailed CCE flow monitoring dataset, how do turbidity currents initiate in Monterey Canyon? Then, how are these flows related to major external events, and what is the control on turbidity current activity in Monterey Canyon? Finally, we then compare results across different settings, scales and grain sizes of turbidity current systems to propose a new model for preconditioning and flow triggering which can be tested by future studies. We conclude by discussing the wider implications of this new model for offshore geohazard assessments.

2. Background

Monterey Canyon is located offshore California on the tectonically active North American-Pacific Plate Boundary (Greene, 1990). The head of Monterey Canyon lies within 100 m of the coast and extends over 300 km offshore to water depths in excess of 4,000 m (Fig. 2; Smith et al., 2005). The Salinas, Pajaro and San Lorenzo Rivers flow into Monterey Bay (Fig. 2). The Pajaro and San Lorenzo Rivers are detached from the head of Monterey Canyon, providing minor direct sediment input. The Salinas River is engineered to enter Monterey Canyon directly under low flow conditions, and discharges $\sim$130,000 $m^3\,yr^{-1}$ of suspended sand. However, the majority of sediment transport occurs during elevated river discharge (Gray et al., 2015). As a result, 95% of Salinas River sediment discharge enters Monterey Bay 6.7 km to the south of the canyon head (Watson et al., 2003; Casagrande and Watson, 2003).

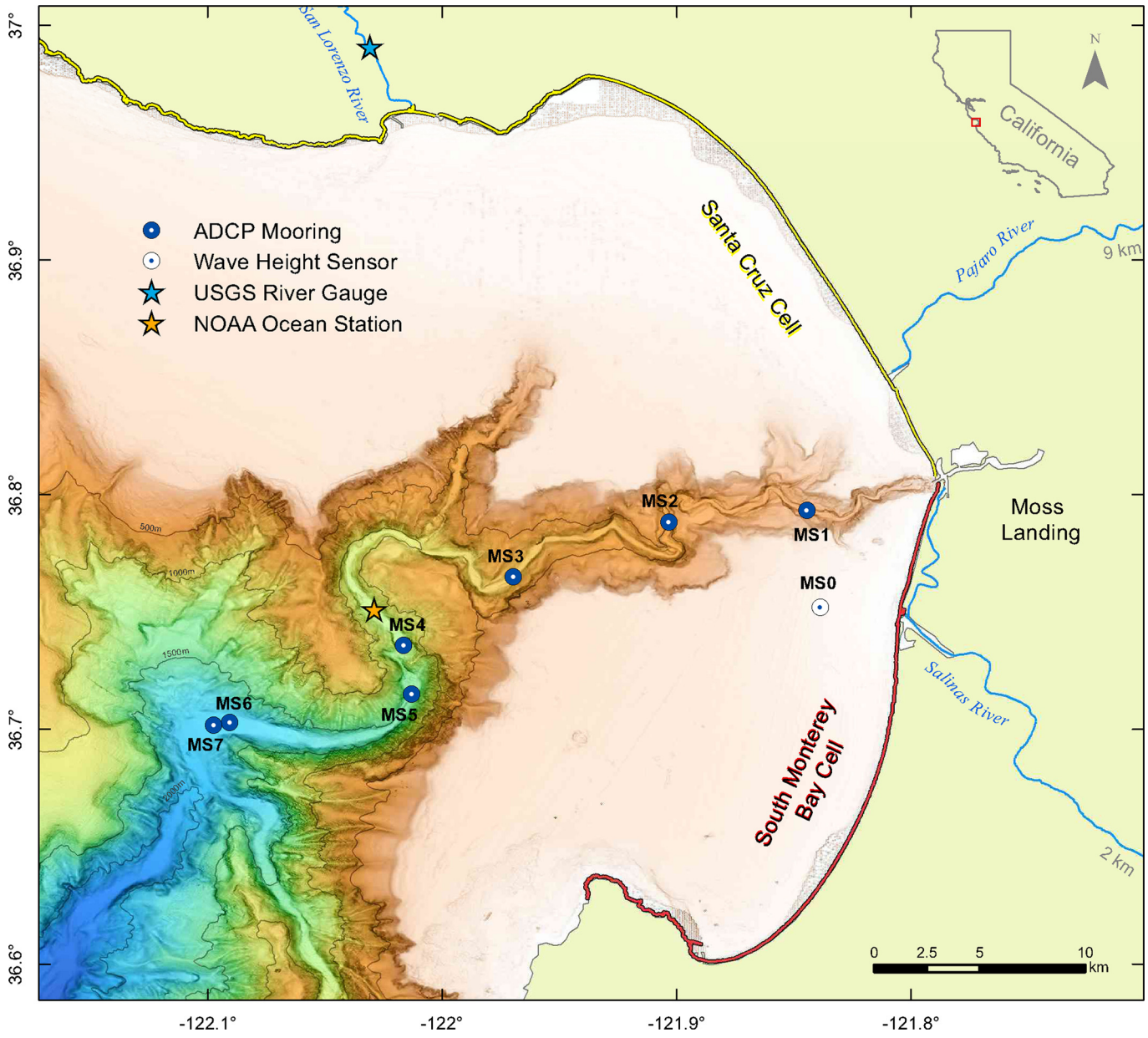

Fig. 2. Monterey Canyon situated offshore California, USA. Map shows mooring locations (MS1-7) and the wave height sensor (MS0) deployed during the CCE. The locations of NOAA metocean buoy and USGS river gauges also shown for San Lorenzo River. Distance labels on Pajaro and Salinas Rivers refer to distance upstream to gauging station beyond the edge of the map. Locations of the Santa Cruz (yellow) and South Monterey Bay Cells (red) are labelled with arrows for the coastal direction of littoral transport. (For interpretation of the colours in the figure(s), the reader is referred to the web version of this article.)

Sediment from the Salinas, Pajaro and San Lorenzo Rivers instead feeds littoral cells entering Monterey Canyon through longshore drift (Farnsworth and Warrick, 2007). The Santa Cruz cell provides >200,000 $m^3\,yr^{-1}$ (Fig. 2; Eittreim et al., 2002) of sand, with an additional 300,000-800,000 $m^3\,yr^{-1}$ of sand from the South Monterey Bay cell (Fig. 2; Willis and Griggs, 2003; Thornton, 2016). Sediment transport is highest during the winter, as the most energetic waves approach from the north-west, diminishing during summer when swells from the south prevail (Patsch and Griggs, 2006).

Direct monitoring and deposit analysis show sediment is primarily transported down-canyon by frequent turbidity currents. Multiple turbidity currents each year runout through the upper 52 km of the canyon, from ~ 300 m to 1850 m water depth (Paull et al., 2003, 2005, 2010, 2018; Xu et al., 2004). Longer runout flows are much less frequent, with flows only reaching a water depth of ~2800-3500 m every 150-200 years (Stevens et al., 2014). Strong (20-80 $cm\,s^{-1}$) internal tidal flows also transport fine-grained sediment between turbidity current events (Maier et al., 2019).

Several possible triggering mechanisms have been proposed for turbidity currents monitored in Monterey Canyon. Johnson et al. (2001) detected four muddy turbid-water underflows over a 12-year period using a conductivity, temperature and depth (CTD) probe and transmissometer located 7 km from the head of Monterey Canyon. These underflow events correlated with peak discharge of the Salinas River (Fig. 2) and were interpreted as hyperpycnal flows. Turbidity current activity was also determined from the down-canyon movement of 1,000 kg instrument frames in the canyon axis (Paull et al., 2003, 2010). Four transport events occurred in a 16-month period in 2001-2002, with six further events recorded during a 26-month period in 2007-2009. Some events occurred during periods of large surface waves, but others coincided with only moderate sea conditions. In December 2002, Xu et al. (2004) detected two turbidity currents using ADCPs, with du-

rations of 6 hours. These turbidity currents corresponded to the highest sea swells observed during a yearlong deployment. However, this same experiment detected two other flows with similar velocities in March and November 2003, which did not coincide with storms, or earthquakes or floods. The relative importance of external triggering mechanisms, and the nature of the resultant turbidity currents, therefore remains poorly understood due to the limited number of events monitored.

3. Data and methods

3.1. The coordinated canyon experiment

Here we report results from the Coordinated Canyon Experiment that included an array of moorings (labelled MS0 to MS7 in Fig. 2) and other instruments, deployed during an 18-month period from October 2015 to April 2017. Instruments were placed within the upper 52 km of Monterey Canyon in water depths of up to 1,850 m (Fig. 2; Paull et al., 2018). Moorings MS1-to-MS5 and MS7 each held a downward-looking 300 kHz ADCP located ~65 m above the seafloor. ADCPs measured profiles of water column velocity and backscatter (proxy for suspended sediment) at 1 m vertical intervals at 30-second resolution. No ADCP measurements were made at MS1 from 15th January 2016 until redeployment on 1st April 2016, as the MS1 mooring broke loose during a powerful turbidity current (Paull et al., 2018). The ADCP at MS4 failed between April-October 2016. Moorings MS1-3 and MS5 included temperature and pressure sensors. A wave height and direction sensor (MS0) was moored outside the canyon to record surface ocean conditions. Small boulder-sized packages with inertial navigation sensors (benthic event detectors, BEDs) were deployed in the upper canyon to measure movement within turbidity currents (Paull et al., 2018).

3.2. Turbidity current timing and runout

A turbidity current is defined here as an event which results in an abrupt increase in ADCP backscatter and down-canyon velocity. The arrival of a turbidity current at each mooring was also accompanied by an increase in pressure as the mooring is tilted towards the seabed. Movement of the mooring during an event separates turbidity currents from powerful internal tides, which can also show a sudden increase in ADCP backscatter and (up and down-canyon) velocity. Minimum flow runout is calculated through successive detection at moorings along the canyon thalweg. The movement of BEDs within the channel axis were used to calculate the initiation time of turbidity currents in the 77 days during which mooring MS1 was out of the canyon. During that time, the sequential movement of BEDs in the upper canyon is interpreted as recording a turbidity current (Paull et al., 2018).

3.3. Measuring potential triggering mechanisms

We analyse the role of the following variables in triggering turbidity currents: earthquakes, wave energy and direction, storm surges, river discharge, and surface and internal tides (10 m above bed). The timing and magnitude of earthquakes are from U.S. Geological Survey (USGS) Earthquake Hazards Program (https://earthquake.usgs.gov/earthquakes/search). Wave height, period and direction, and sea surface height are recorded at MS0 every two hours. Here we calculate an indication of wave energy as,

$$Wave\ Energy = \frac{1}{8}\rho g \mathrm{H}^2 \mathrm{L}.$$

Where ρ is water density, g is acceleration by gravity. H refers to significant wave height and L is mean wavelength derived from wave period through the wave dispersion relation (Dean and Dalrymple, 1991) recorded at MS0. The longshore component of wave energy is directly proportional to the longshore transport rate of sand (Komar and Inman, 1970). Internal tide signals are obtained from mooring data at MS1 with 30-second resolution. Data were binned and averaged over 10-minute intervals, with measurements related to turbidity currents removed. The bin prior to turbidity current detection was taken as the conditions during the event. Hourly air pressure measurements at National Oceanic and Atmospheric Administration (NOAA) Station 46092 (https://www.ndbc.noaa.gov/) provide an indication of potential storm surges. USGS stream gauges 11152500, 1159000 and 11161000 provide daily average discharge for the Salinas, Pajaro and San Lorenzo rivers (Fig. 2; https://waterdata.usgs.gov/nwis/rt). Suspended sediment concentrations were estimated for the Salinas, Pajaro and San Lorenzo rivers using established rating curves (Johnson et al., 2001).

The time of turbidity current detection at MS1 (or initial BED transport) is taken as the point of flow initiation for comparison to potential triggering variables. As a result, there is some uncertainty in the exact timing of flow initiation. Most flows were first detected at MS1 (~300 m water depth), therefore flows may have originated anywhere between MS1 and the canyon head. Assuming turbidity current velocity is $>2\ m\,s^{-1}$ following initiation to detection at MS1 (or shallowest BED), the transit time from any point in the canyon head will be <1 hour and therefore above the resolution of wave energy and direction, storm surges, river discharge, and surface tide measurements. Greater uncertainty arises when comparing event initiation to internal tide velocity.

3.4. Statistical comparison of triggering variables

The following criteria are used to analyse variation between event and non-event conditions to assess the influence of individual triggers throughout the CCE. We calculate the difference between medians (DBM) as a percentage of overall visual spread (OVS), where OVS is the range from the lowest to highest interquartile (25th and 75th percentile) range (e.g. Rao and Liu, 2017). The number of events in this study (N = 14) is insufficient for complex statistical analysis; however, calculating DMB as a percentage of OVS provides a quantification of distribution offset between event and non-event conditions for each of the hypothesised explanatory variables.

3.5. Comparative datasets from river-fed systems

We compare our results from Monterey Canyon with previously published observations from two other well-monitored submarine systems for which we provide further details in Supplementary Table S1. As far as we are aware, these are the only other sites where the timing of numerous turbidity currents (>10-100) have been measured precisely via direct monitoring. However, in each case the duration of direct monitoring is <18 months, such that more infrequent events may not be well captured.

The first location is Squamish Delta in Howe Sound, British Columbia, which is fed by a sand-dominated and relatively small (200-1,000 $m^3\,s^{-1}$) discharge river. At this location, 106 turbidity currents were recorded in 2011 from repeat seafloor surveys and ADCP measurements (Hughes Clarke et al., 2014; Clare et al., 2016). The second location is the upper mud-dominated Congo Canyon, offshore West Africa. This system is fed by the Congo River, the second largest (40,000-60,000 $m^3\,s^{-1}$) discharge river on Earth (Milliman and Meade, 1983). The timing of turbidity currents in the Congo Canyon was measured using two methods. Especially powerful flows were recorded by cable breaks between 1893 and 1932 (N = 23), close to the coast (Heezen et al., 1964). ADCP

Table 2
Statistical metrics to compare the distribution variation of potential triggering mechanism conditions with background conditions observed during the CCE. We calculate the difference between medians (DBM) as a percentage of overall visual spread (OVS), where OVS is the range from the lowest to highest interquartile range (e.g. Rao and Liu, 2017). Results are ranked in order of their statistical importance for triggering flows.

Triggering variable	Event median	Background median	Difference between medians	Overall visual spread	DBM/OVS (%)
Wave Energy [$\times 10^4$ J m^{-2}]	4.2	1.6	2.6	6.2	41.9
Air Pressure [mbar]	1012.5	1017.3	4.8	14.4	33.7
Water Level [m from mean]	0.1	0.0	0.1	0.9	17.2
Combined River Discharge [m^3 s^{-1}]	25.6	2.2	23.4	202.3	11.6
Internal Tide Velocity [m s^{-1}]	−3.4	−2.6	0.8	23.8	3.2
Salinas River Discharge [m^3 s^{-1}]	0.0	0.0	0.0	0.6	0.0

moorings at sites ~150 km from the coast record sufficiently long runout flows (N = 10; Azpiroz-Zabala et al., 2017; Simmons et al., 2020). Data from these two comparative sites allow us to compare patterns of flow timing in diverse physiographic settings with different sediment delivery mechanisms and grain sizes.

4. Results

4.1. Source, number and character of events in Monterey Canyon

During the 18-month monitoring period, fourteen flows initiated in upper Monterey Canyon in water depths of <300 m (Fig. 3A). Eleven turbidity currents were detected using MS1 and three based on movement of BEDs. Turbidity currents detected during the CCE have frontal (transit) velocities of up to 7.2 m s^{-1}. Three flows ran out through the entire instrument array, for at least 52 km along the canyon thalweg (Paull et al., 2018).

4.2. Correlating environmental variables with turbidity current timing in Monterey Canyon

We now consider the relationships between the 14 turbidity currents that initiated in upper Monterey Canyon, and factors that may have triggered the flows. We first determine the potential triggering mechanisms (Fig. 1) that occurred during the period of instrument deployment in Monterey Canyon. Of the potential triggering mechanisms we analyse how each correlates to turbidity current timing.

4.2.1. Earthquakes

Several small earthquakes, with magnitudes of up to 4.2 M_W, and epicentres within 100 km of the canyon head, were detected during the CCE. However, these earthquakes did not coincide with any turbidity currents (Fig. 3A). Therefore, small earthquakes did not trigger any flows in Monterey Canyon during the deployment period.

4.2.2. Storms – large waves and storm surges

A storm is defined as a period of large, high-energy waves, low air pressures and strong winds. The compound effect of these factors may also result in a storm surge. Wave energy and air pressure (+42% and −34% DBM/OVS respectively; Table 2) were the triggering variables with the largest offset between event and background conditions. 65% of turbidity currents occur when wave energy was above the 70th percentile of its annual range (Figs. 3C, S1). The five largest depressions in air pressure also all correspond to times of turbidity current activity (Figs. 3D, S1). However, not all periods of high wave energy and significant wave height correspond to a turbidity current. Periods with some of the highest wave energy (up to 4.2×10^5 J m^{-2}), significant wave heights and periods (up to 6 m and 13 seconds; Fig. S2) did not include any turbidity current activity (Figs. 3C, S1). Similarly, not all turbidity currents occurred during depressions (Fig. 3D). Turbidity currents were typically detected at the onset of storms, when wave energy starts increasing rather than at individual peaks (Fig. 4). Wave direction measured at MS0 was almost exclusively from the north-west during the CCE, even during summer. Two turbidity currents were detected on rare days of south-west approaching storm waves (Fig. 3B).

4.2.3. River floods

The combined discharge from the Salinas, Pajaro and San Lorenzo Rivers remained below 10 m^3 s^{-1} for 80% of the deployment period. In fact, six turbidity currents were detected during a period when the combined river flow was <3 m^3 s^{-1} (Figs. 3E, S1). There is a trend to higher combined discharge during events (+12% DBM/OVS; Table 2), but this is skewed by the elevated discharge during January-February 2017. During this period the Salinas, Pajaro and San Lorenzo discharge is the highest observed during the CCE with an abnormal transition from being almost completely dry to moderate discharge (Figs. 3E, S1). However, the Salinas River shows no change in median value between events and background conditions (Table 2). Elevated river discharges also correlated strongly with storms that caused greater wave energy, or larger wave heights. Turbidity current timing usually preceded peak river flooding. This is most visible when compared to Salinas River discharge. Here, seven events occur within a five-day window of discharge elevation, yet only three turbidity currents are preceded by any substantial river discharge (Figs. 3, 4, S1).

4.2.4. Sea surface and internal tides

Sea surface water level conditions during events show a minor trend to high waters (+17% DBM/OVS; Table 2). However, turbidity currents are detected at all stages in the tidal cycle (Figs. 3F, S1). Measurements of internal tide velocities were recorded for 11 events, and seven of these coincide with down-canyon flowing internal tides immediately preceding the event (Figs. 3G, S1). The distribution of internal tide velocity concurrent with turbidity currents, however, shows almost no variation (3% DBM/OVS; Table 2) with measurements throughout the CCE.

4.3. Clustering of turbidity current activity in Monterey Canyon

Increases in wave energy and decreases in air pressure during storms display the greatest offset in event to background measurements. However, changes in these variables are not robust predictors of turbidity current activity. What is clear, however, is that turbidity currents are most frequent during the winter months (13 of 14 events; shaded region Fig. 3). Throughout the winter, wave energy (a proxy for sediment supply to the canyon head) is also highest. Using the DBM/OVS method, wave energy during 2016 shows a 47% increase during November-March from April-October.

The cumulative wave energy between events (black circles; Fig. 3C) is consistent, with each of the 13 events triggered during the winter occurring within an order of magnitude (mean 9.8×10^6 J m^{-2}, standard deviation 4.7×10^6 J m^{-2}). The single event initiating outside the winter (1st September 2016) occurred after cumulative wave energy of 3.9×10^7 J m^{-2}, which is four times higher than the mean value between winter events.

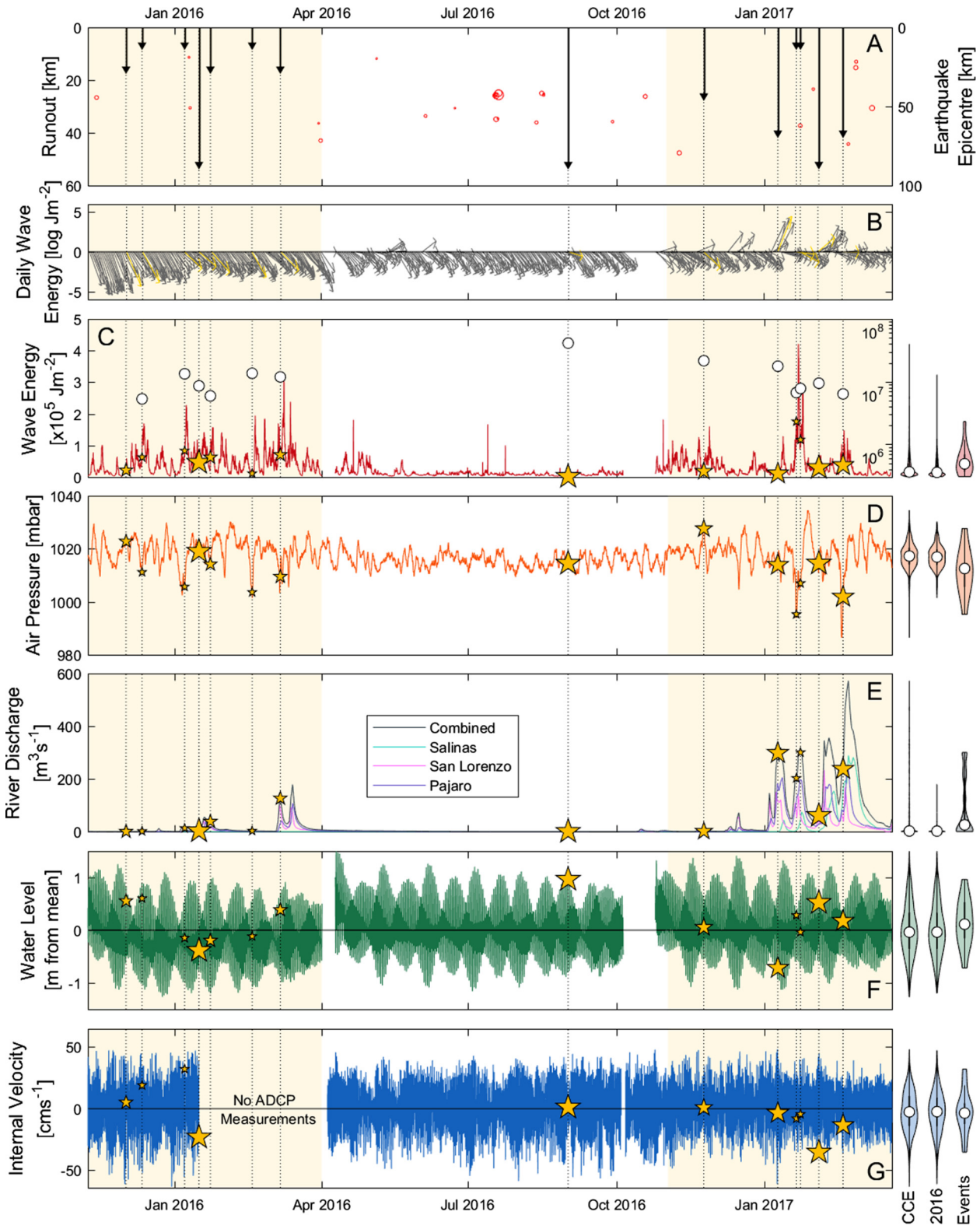

Fig. 3. Time series during CCE of event occurrence and triggering variables discussed. Dotted lines in all panels indicate when turbidity currents occur. (A) The timing of detected turbidity currents and runout distance down-canyon (left); and the timing of earthquakes with epicentres within 100 km of Moss Landing, data point size relative to magnitude (right). (B) Mean daily wave measurements where arrow length represents wave energy and direction denotes wave direction, yellow arrows display conditions on days with events. Arrow heads point to direction of wave motion. (C) Red line shows wave energy and white-filled circles indicate the cumulative wave energy since the previous flow. Yellow stars in C-G show the conditions of each variable during events, the size of star is relative to flow runout. (D) Air pressure measured from NOAA Buoy 46092 located 54 km offshore from Moss Landing, California. (E) River discharge from USGS gauges closest to the mouths of the San Lorenzo, Pajaro and Salinas Rivers, with combined flow. (F) Deviation of water level from mean during CCE measured from wave height sensor. (G) Internal tide velocity measured at MS1 10 m above bed. Data were binned and averaged over 10-minute intervals, with measurements related to turbidity currents removed. Shaded area in A-G shows period of turbidity current clustering in the November-March winter storm season. Violin plots adjacent to C-G show the distribution and range of conditions of each triggering variable throughout the CCE, 2016 and during events. White filled circle shows mean value for each data set and the thick central black line represents the interquartile range. Gaps in wave, water level and internal velocity data are a result of instrument turnover.

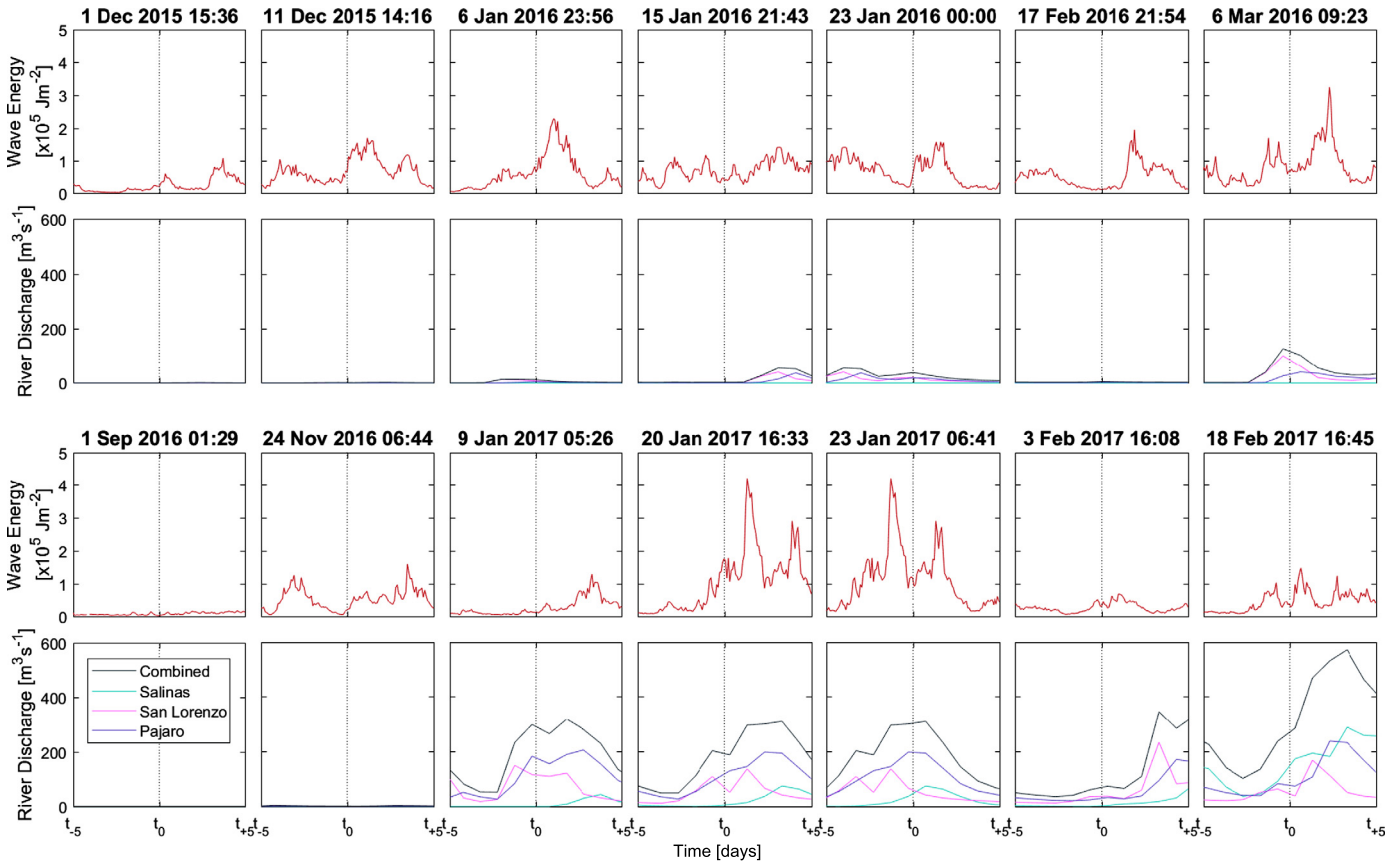

Fig. 4. Measurements of wave energy (red) and San Lorenzo, Pajaro and Salinas Rivers discharge (blue shades), with combined flow (grey) five days prior and following turbidity currents initiating in the upper canyon during the CCE. Central dotted line in each plot indicates the first detection of turbidity current.

5. Discussion

This section now discusses how preconditioning and triggering mechanisms relate to turbidity current activity. First, we discuss how flows initiate in Monterey Canyon. Then, we assess the role of antecedent conditions prior to events recorded during the CCE, i.e. preconditioning factors, and how these are linked to turbidity current timing and triggering. Finally, we compare results from Monterey Canyon to directly monitored turbidity currents in other systems, and propose a model for the preconditioning and triggering of flows.

5.1. How do turbidity currents initiate in Monterey Canyon?

Initiation of the observed turbidity currents by plunging (hyperpycnal) river floods, or relating to surface plumes is inconsistent with data from Monterey Canyon. During our study period, the nearby rivers did not exceed the water discharge threshold of 300 $m^3\,s^{-1}$ (Fig. 3E) predicted to generate hyperpycnal flow (Johnson et al., 2001). Moreover, the long distance from the canyon head to the mouths of the Pajaro (5 km) and San Lorenzo Rivers (26 km) does not favour initiation through sediment settling from river plumes (e.g. Parsons et al., 2001), and sediment would likely be dispersed by along-shelf currents (Rosenberger et al., 2016) and waves before settling in the canyon head. Additionally, it is improbable that the turbidity maximum will reach the canyon head 100 m offshore, therefore tidally controlled flow initiation (Hage et al., 2019) is unlikely to apply here. Thus, variations in river discharge are unlikely triggers for the observed turbidity currents.

The head rim of Monterey Canyon progrades and fails on a sub-annual cycle, with an estimated 140,000 m^3 of sediment evacuated annually from the rim of the canyon head and re-deposited locally along the canyon axis (Smith et al., 2005, 2007). Repeat mapping by Smith et al. (2005, 2007) showed a minimum (i.e. Vendettuoli et al., 2019) sediment volume of ~260,000 m^3 accumulated over six months (September 2002 to March 2003). This included a sediment wedge (~70,000 m^3) located near the Moss Landing Harbour mouth resulting in 10 m seaward propagation and >2 m aggradation of the canyon head-rim. This sediment wedge then failed between September 2003 and September 2004, when a total of 230,000 m^3 of sediment was evacuated. This period of sediment loss coincided with a turbidity current recorded using ADCPs at 1450 m water depth in November 2003 (Xu et al., 2004). It is likely that some or all of this reported sediment loss in the canyon head is the source of this monitored turbidity current. Therefore, it is conceivable that other turbidity currents, such as those observed during the CCE, are related to the disintegration of sediment failures along the rim of the canyon head.

5.2. What preconditions and triggers slope failure in Monterey Canyon?

During our study period no single obvious triggering mechanism was observed to cause flow initiation at Monterey Canyon. Turbidity currents during the CCE did not coincide with earthquakes, though it is important to note that all earthquakes that occurred during instrument deployment were of small (4.2 M_W) magnitude. Our observations show that higher wave energy (+42% DBM/OVS) and lower air pressure (−34% DBM/OVS; Fig. 3; Table 2) increase the likelihood of turbidity currents. However, the most energetic waves during our study, and previous Monterey Canyon

monitoring (e.g. Paull et al., 2003; Xu et al., 2004), did not always generate turbidity currents. Moreover, some turbidity currents initiated during periods of only moderate wave energy (Figs. 3, 4). Increased discharge of the Salinas River also shows no significant correlation with turbidity currents (Table 2). Additionally, the three turbidity currents that coincided with Salinas River discharge >1 $m^3\,s^{-1}$, all preceded peak river discharge (Fig. 4). Turbidity current initiation at all points of sea surface level and internal tides (Fig. 3) show that tides are also not a consistent triggering mechanism during the CCE.

A seasonality in turbidity current activity is apparent though, with flows clustering during the winter (13 of 14 events; shaded region Fig. 3). Throughout the winter, sediment supply to littoral cells from rivers is elevated (Fig. 3E) and more energetic waves then result in increased longshore transport (Fig. 3C), thereby trapping and depositing sediment within the canyon head (Smith et al., 2005, 2007). The volume of sediment entering the canyon head can be estimated using wave energy as a proxy for littoral sand transport (Komar and Inman, 1970). Notably consistent values of cumulative wave energy are observed between these winter turbidity currents (Fig. 3C), suggesting a similar volume of sediment enters the canyon head between events. Such consistent cumulative sediment volumes cannot be reproduced by randomly generating the timing of turbidity currents throughout the monitoring period (Fig. S3).

The increased rate of sediment supply and accumulation in head of Monterey Canyon during the winter favours turbidity current activity. Submarine slope failures have been linked to periods of enhanced sediment deposition and failure from either slope over-steepening and retrogressive failure known as 'breaching' (Van Den Berg et al., 2002; Mastbergen and Van Den Berg, 2003) or the development of high excess pore pressures and liquefaction (e.g. Christian et al., 1997; Flemings et al., 2008). Both failure mechanisms are capable of producing turbidity currents, however breaching usually produces more sustained flows (Mastbergen and Van Den Berg, 2003) than those observed during the CCE (Paull et al., 2018).

Direct measurements of pore pressure were not made during the CCE, or in any other sand-rich submarine canyon to date. However, we propose that rapid accumulation of sediment along the head-rim of Monterey Canyon during the winter led to elevated pore pressures, thereby preconditioning failure. Excess pore pressures arise where pore fluid cannot dissipate quickly enough due to low permeability along drainage paths, which in turn undermines the shear strength and slope stability. Rapid deposition and thicker volumes of sediment therefore favour slope failure (e.g. Dugan and Sheahan, 2012). We note that development of excess pore pressures can also depend on factors other than the total sediment volume supplied. The time-scale over which excess pore pressures are sustained (therefore the period a slope remains preconditioned) or dissipate is controlled strongly by the sediment grain-sizes and hydraulic conductivity. Consolidation coefficients (c_v) vary over multiple orders of magnitude depending on small changes in fine-mud fraction, as well as density changes between granular layers of equivalent grain size (Major and Iverson, 1999; Iverson, 2005; Özener et al., 2009; Fig. 5). For instance, an additional loading of 10 m sediment thickness will require weeks for pore pressures to dissipate in clean sandy systems (e.g. $c_v \approx 10^{-4}$). However, excess pore pressures may persist for several months when mud is added ($c_v \approx 10^{-5}$), or last for several years in a muddy delta system ($c_v \approx 10^{-6}$; Fig. 5; Bennett and Faris, 1979), and may be exacerbated by other effects such as tidal loading-unloading cycles (Christian et al., 1997) or where a hydraulic link exists between onshore and offshore aquifers (e.g. Stegmann et al., 2011). The presence of organic material (that may degrade to release biogenic gases) can also result

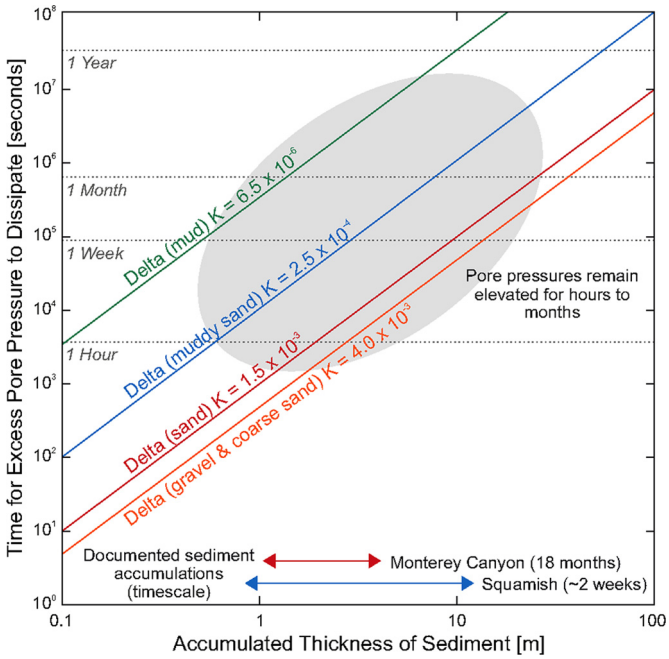

Fig. 5. The role of grain size and sediment supply on the period of system preconditioning demonstrated by hydraulic conductivities in a range of delta systems from Fleckenstein et al. (2006). Demonstrating time for excess pore pressures to dissipate to 1/E (37% of initial value). Clare et al. (2016) show up to 12 m aggradation within 1 week on the delta lip at Squamish, Smith et al. (2005, 2007) a 8 m aggradation at the head of Monterey Canyon over months.

in elevated pore fluid pressures (e.g. Christian et al., 1997). Deposition of organic debris including macroalgae occurs throughout the year in Monterey Canyon, becoming most abundant during spring/summer (Okey, 1997; Harrold et al., 1998). While this is the period when turbidity currents are least frequent in Monterey Canyon (Fig. 3), degradation of that organic debris will take months (de Bettignies et al., 2020). Thus, there is a balance between build-up of excess pore pressure during periods of more rapid sediment supply, gradual pore pressure dissipation between pulses of storm induced sediment input, and other influences on subsurface pore pressures such as biogenic gas formation. The exact location of sediment deposition is also unknown as we lack repeat seabed surveys over short enough timescales, including along the canyon head-rim; time-lapse surveys from Autonomous Underwater Vehicles were undertaken along the canyon axial channel during the CCE, but only every ~3 months (Paull et al., 2018).

Only one turbidity current initiated outside the winter months (1st September 2016) when average littoral transport rates to the head of Monterey Canyon were lower (Fig. 3C). The event was initially relatively weak (velocity of 3 $m\,s^{-1}$ and <10 m thick), but the flow became much more prolonged and faster mid-canyon. Between MS3 and MS5 (Fig. 2) the turbidity current thickened to >20 m and accelerated to >4 $m\,s^{-1}$ before running out through the entire CCE instrument array (Heerema et al., 2020). Similar to turbidity currents initiating in the winter, no exceptional external mechanism is apparent during, or immediately preceding, this anomalous event (Fig. 3). However, this flow did occur following the greatest cumulative build-up in wave energy of all recorded events, over four times higher than the mean between winter turbidity currents (Fig. 3C). This represents the highest volume of estimated sediment accumulation in the canyon head prior to turbidity current initiating during the CCE. Such large volumes of sediment are capable of generating excess pore pressures. The rate of pore pressure dissipation is also likely reduced outside the winter through densification and the deposi-

tion of a surficial mud layer (Paull et al., 2013; Heerema et al., 2020) resulting in vertical sediment heterogeneity (Özener et al., 2009).

In the absence of a consistent external variable correlating with the timing of flows, turbidity current activity during the CCE is better related to preconditioning factors, rather than an individual instantaneous trigger. We propose a window of enhanced turbidity current activity is set up during the winter storm season, following an increased rate of sediment supply to the head of Monterey Canyon (shaded region Fig. 3). Here rapid sediment deposition generates excess pore fluid pressures preconditioning slope failure. Where excess pore pressures cannot fully dissipate, the canyon head can remain preconditioned for several days or weeks. As such, it is possible for delays to exist from initial peaks of sediment input and the timing of a turbidity current. Diminished sediment transport rates outside the winter reduce the build-up of pore pressures, therefore periods where the slope is preconditioned are rarer. However, sufficiently large volumes of sediment deposition (as observed prior to the 1st September 2016 event) can still generate excess pore pressures to precondition failure outside the window of enhanced turbidity current frequency. In both cases, once the slope is preconditioned a large external triggering mechanism is not a requirement for turbidity current initiation. Rather minor perturbations in antecedent conditions, most likely local pore pressure variation as a result of wave loading, are capable of triggering failure.

5.3. A common pattern of seasonal increases in turbidity current activity

A common pattern of seasonal increases in turbidity current activity emerges in systems where numerous (>10-100) flows have been precisely measured through direct monitoring. Turbidity currents in Monterey Canyon (a sandy canyon-head system fed by littoral drift), the Squamish Delta (a sandy river-fed fjord-delta) and the Congo Canyon (a muddy system fed by an exceptionally large river) are all most frequent when sediment supply is highest, regardless of setting, grain size or delivery mechanism (Fig. 6).

In sand-rich littoral-fed canyons, such as Monterey Canyon and other systems along the Californian Margin (Inman et al., 1976; Paull et al., 2003, 2010, 2018; Xu et al., 2004, 2010; Puig et al., 2004), Nazaré Canyon, offshore Portugal (Martín et al., 2011) and canyons in the Gulf of Lions, Mediterranean (Canals et al., 2006), turbidity current activity is focussed in the winter storm seasons, where sediment transport to canyon heads is highest. Turbidity currents still occur outside this period, but are much less common (Fig. 6a).

Systems where rivers directly supply sediment are most active during periods of elevated river discharge. For example, turbidity current activity is strongly seasonal at Squamish Delta, with intense activity switching on during periods when river discharge exceeds $\sim$ 300 $m^3\ s^{-1}$ (Fig. 6b; Hughes Clarke et al., 2014; Clare et al., 2016). Here single monitoring campaigns have recorded >100 individual flows, which primarily occur within the spring/summer freshet season when glacial melting increases river discharge for $\sim$4 months (Fig. 6b). Turbidity currents rarely correlate with peaks in river discharge. Instead $\sim$25% of flows initiate through slope failure following hours to days delays after rapid deposition on the delta-top, typically at low tide. The remainder of turbidity currents are linked to settling of surface plumes (Clare et al., 2016; Hizzett et al., 2018; Hage et al., 2019). Historical cable breakages related to turbidity currents offshore from the mouths of the Congo and Magdalena Rivers and within the Gulf of Corinth are also most frequent during periods of elevated river discharge (Heezen et al., 1964, 1966). However, in very large river systems with complex catchments, turbidity currents may show less clustering. For example, the Congo River hydrograph comprises of two broad discharge peaks where turbidity current activity is increased (Fig. 6c; Heezen et al., 1964; Azpiroz-Zabala et al., 2017; Simmons et al., 2020).

5.4. New model for preconditioning and triggering of turbidity currents via slope failure

We combine insights from Monterey Canyon and these other field sites (Fig. 6) into a generalised model for turbidity current activity in areas of sustained sediment accumulation, such as canyon-heads or river mouths. The model assumes that initiation occurs via slope failure, and it is thus not applicable where turbidity currents are triggered primarily in other ways, including hyperpycnal or surface river plumes (Fig. 1). The model explains why some flows do not coincide with major external triggers, or variable time delays occur between flows and those major external triggers, as well as seasonal increases in flow activity that follow fluctuations in sediment supply. It is hoped that future work can then test the model more rigorously, including its basic assumptions regarding triggering via slope failure, and persistence of excess pore pressures long after peak sedimentation rates. Unfortunately, at present, there are no suitable time series of excess pore pressure available for such a purpose.

In this model, rapid or sustained sediment deposition causes elevated excess pore pressure in the subsurface. Pore pressures can be further elevated when links exist between onshore and offshore aquifers (e.g. Stegmann et al., 2011), tidal loading-unloading cycles or the presence of organic matter (Christian et al., 1997). The generation of these excess pore pressures preconditions slopes such that they are close to failure (Fig. 7a). Here, small final perturbations can thus trigger slope failure and a subsequent turbidity current (Fig. 7b). For example, this may arise from further changes in the pore pressure regime due to cyclic wave loading, tidal variations, elevated bed shear stresses arising from dense water cascading and internal tides or a combination of these factors (Fig. 1). Large sediment accumulations in the system head and upper reaches may also be entrained within a flow, whereby an initial relatively small event may ignite into a much greater volume, and longer run-out flow (e.g. Piper and Savoye, 1993; Hizzett et al., 2018; Heerema et al., 2020). A broad analogy may be drawn with snow avalanches, which can be triggered by progressive snow accumulation, without a major external trigger, although there are also significant differences between snow pack and sediment structures.

The model implies that excess pore pressures take time to accumulate and build along weaker horizons, or eventually dissipate. This can result in time-delays between individual peaks in sediment supply and the timing of slope failure and initiation of turbidity currents. Most commonly, time delays are short (hours to weeks), such that turbidity current activity occurs primarily during specific seasons with elevated sediment supply. However, longer delays can sometimes also occur, as pore pressures persist for longer, or a cumulative sediment supply volume is reached to precondition slopes. In these cases, powerful and long runout turbidity currents occur during periods of low sediment supply, as occurred on 1st September 2016 in Monterey Canyon.

5.5. Wider implications for geohazard assessment

Although not observed during our study of Monterey Canyon, turbidity currents can clearly be caused by major external triggers, including major earthquakes, typhoons and river floods. This was famously shown by the 1929 Grand Banks event, where a 7.2 M_W earthquake-triggered a turbidity current, recorded by sequential cable breaks extending up to 720 km offshore (Heezen and Ewing, 1952; Piper et al., 1999). More recently, the 2016 7.8 M_W

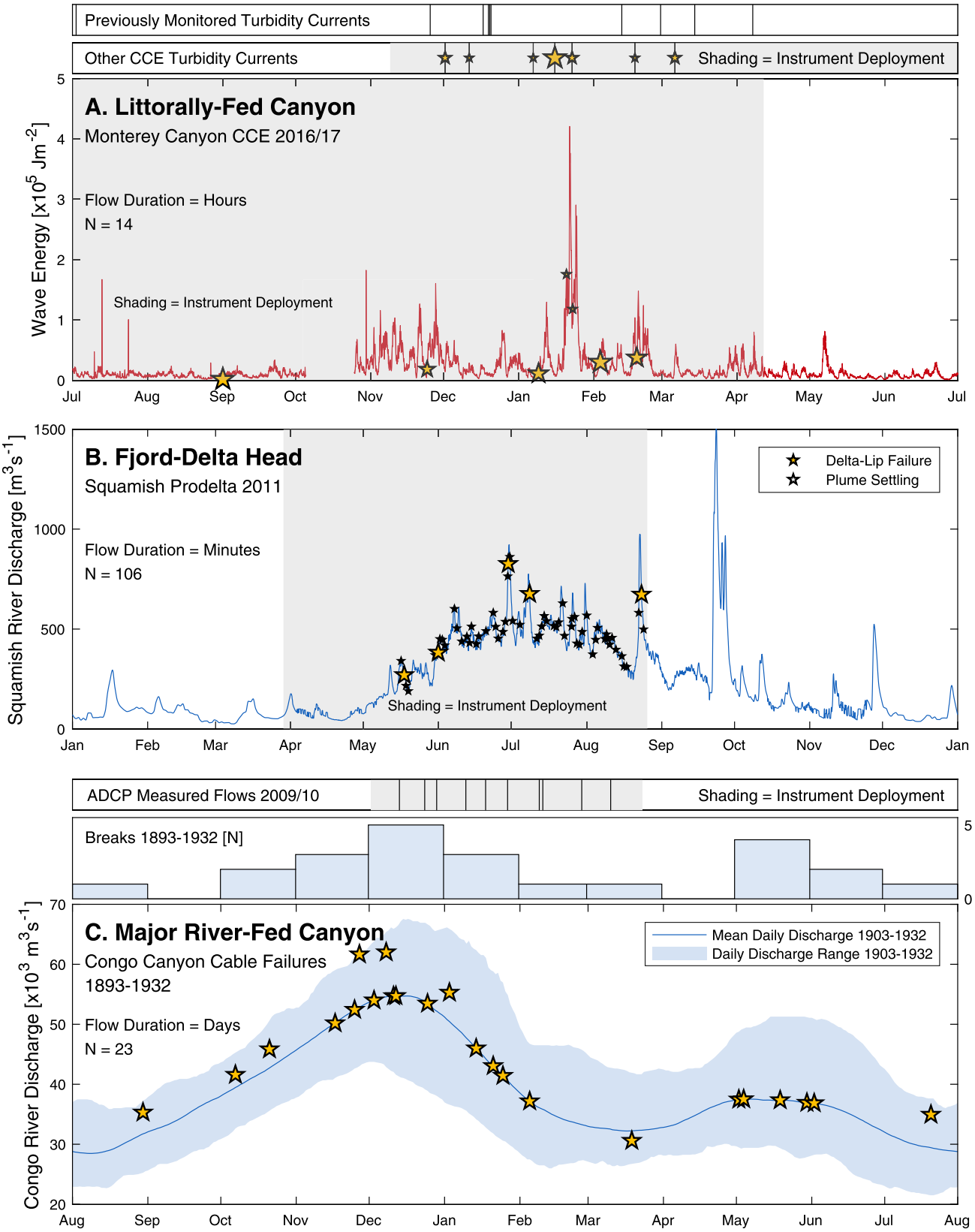

Fig. 6. Comparison of annual turbidity current timing in different physiographic settings and sediment delivery mechanisms. (A) Monterey Canyon as an example of a littoral-fed canyon showing events from July 2016 to June 2017 during the CCE. Stave above plot shows the day and month of previously measured flows by Paull et al. (2003, 2010) and Xu et al. (2004) and other flows recorded during the CCE. (B) Squamish Prodelta, British Columbia, Canada as an example of a submarine channel system connected to a fjord-delta head. Timing and flow initiation shown during 2011 from direct monitoring by Clare et al. (2016). (C) Congo Canyon as an example of a major river-fed canyon. Day and month of historical cable breaks between 1893 and 1932 documented by Heezen et al. (1964). The staves above show the day and month of turbidity currents directly monitored between August 2009 and September 2010 directly monitored by Azpiroz-Zabala et al. (2017) and Simmons et al. (2020) and the number of cable breaks detected by month between 1893 and 1932. Yellow stars in panels show conditions recorded during events. Size of star for turbidity currents during the Monterey CCE relative to runout. For Congo Canyon cable breaks earlier than 1903 stars placed on average Congo River discharge, records prior to 1903 were not available.

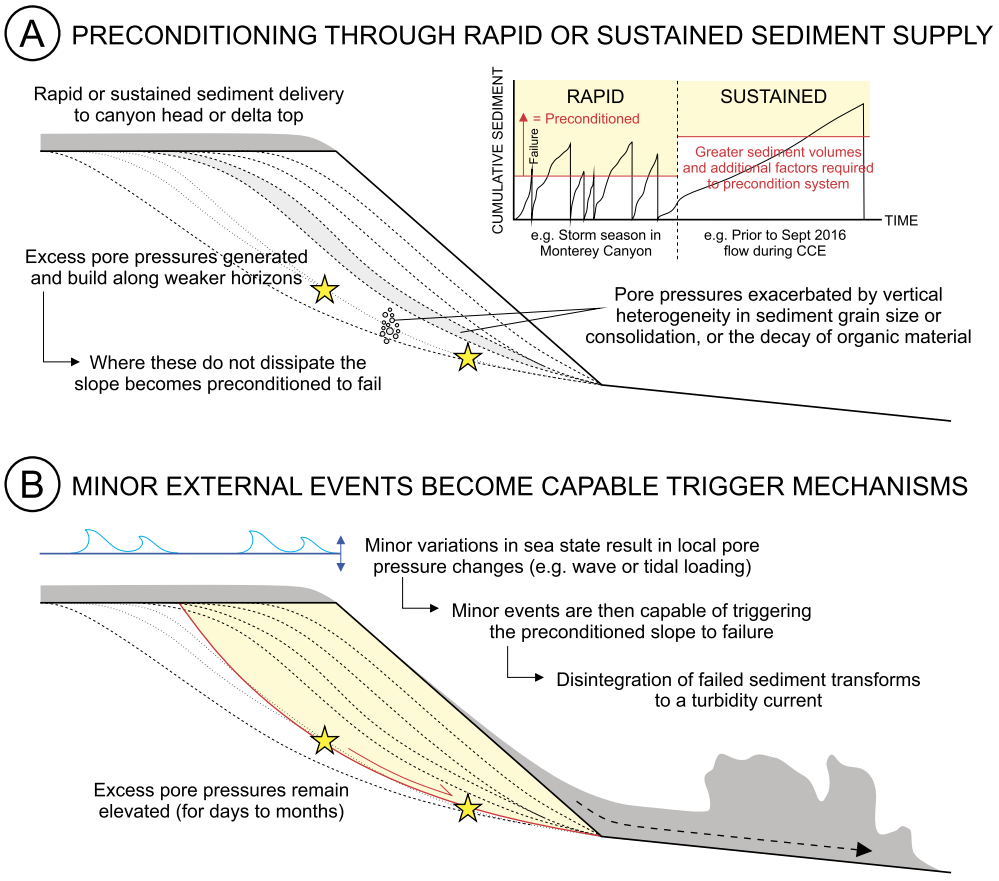

Fig. 7. A new model for turbidity current activity in areas of sustained sediment accumulation, such as canyon-heads or river mouths, where initiation occurs via slope failure. Here (A), rapid or sustained sediment deposition in the system head generates excess pore pressures preconditioning the slope to failure. Where pore pressures cannot fully dissipate the slope will remain preconditioned to failure. (B) This allows minor external events to become capable triggering slope failure and a subsequent turbidity current through further changes to local pore pressure.

Kaikōura earthquake, New Zealand, triggered a turbidity current with a runout of >680 km through the Hikurangi submarine channel (Mountjoy et al., 2018). Furthermore, cable-breaking flows in the Gaoping Canyon, offshore Taiwan, in 2006, 2009 and 2010 appear to be triggered by either large ($M_L > 7$) earthquakes, tropical cyclones or river floods (e.g. Hsu et al., 2008; Carter et al., 2012; Gavey et al., 2017; Pope et al., 2017).

However, our results show that relatively powerful (up to 7.2 $m\,s^{-1}$ and long runout >52 km) turbidity currents, can sometimes initiate through slope failure without a major external trigger such as storms, floods or earthquakes. Flows triggered by small external perturbations can move 800 kg objects, and thus could damage cables and seabed infrastructure. Most commonly, increased turbidity current activity occurs during periods of high relative sediment supply, although the precise timing of turbidity currents may not coincide with individual floods or large storm waves. At least in these types of systems, predicting the exact timing of turbidity currents is challenging. However, where sediment supply is seasonal, we can anticipate windows of increased turbidity current likelihood, for geohazard assessments and the routing or maintenance of critical seafloor infrastructure.

6. Conclusions

This study presents some of the most detailed measurements yet for the timing of turbidity currents and environmental conditions that may trigger flows. No consistent trigger was observed for the fourteen flows that were recorded in Monterey Canyon, but turbidity currents were more frequent in the winter storm season. During the winter, heightened wave energy increases sediment transport to the canyon head and similar volumes of sediment were estimated to enter the canyon head between flows. A single powerful (up to 4.8 $m\,s^{-1}$ and >52 km runout) event was observed outside the winter, when sediment supply rate is reduced. However, the total sediment volume entering the canyon head was approximately four times higher than the mean between winter events. We therefore propose that turbidity current activity is better related to sediment supply and slope preconditioning rather than individual triggers.

We combine insights from Monterey Canyon and other sites of direct monitoring to produce a model for preconditioning and triggering of turbidity currents via slope failure, in locations of sustained sediment accumulation such as canyon heads and river deltas. In this model, rapid or sustained sediment supply alone can produce elevated pore pressures, which may persist, thereby predisposing slopes to fail for hours to months (or potentially even longer in muddy systems) after initial sediment deposition. Small perturbations in antecedent conditions resulting in local pore pressure variation then become capable triggers, demonstrating that major external events such as earthquakes, storms or river floods are not a prerequisite for turbidity current activity.

CRediT authorship contribution statement

Lewis Bailey: methodology, analysis, validation, visualisation, writing original draft. **Michael Clare:** analysis, conceptualisation, validation, writing original draft, supervision. **Kurt J. Rosenberger:** analysis, conceptualisation, investigation, writing original draft.

Matthieu Cartigny: analysis, writing original draft. **Peter Talling:** analysis, conceptualisation, writing original draft, funding acquisition. **Charles Paull:** conceptualisation, investigation, review/editing, funding acquisition. **Roberto Gwiazda:** investigation, review/editing. **Daniel Parsons:** conceptualisation, investigation, review/editing, funding acquisition. **Stephen Simmons:** investigation, review/editing. **Jingping Xu:** conceptualisation, review/editing, funding acquisition. **Ivan Haigh:** review/editing, supervision. **Katherine Maier:** investigation, review/editing. **Mary McGann:** investigation, review/editing. **Eve Lundsten:** investigation, data curation, review/editing.

Declaration of competing interest

The authors declare that they have no known competing financial interests or personal relationships that could have appeared to influence the work reported in this paper.

Data availability

Data generated during the CCE are available at https://www.mbari.org/science/seafloor-processes/geological-changes/coordinated-canyon-experiment-datareport-main-page/ and https://www.sciencebase.gov/catalog/item/5a74c1fce4b00f54eb1c828f. More details about data acquisition, including other deployed instruments, are provided by Paull et al. (2018).

Acknowledgements

LPB was supported by the Natural Environmental Research Council as part of the SPITFIRE Doctoral Training Program (Grant Number NE/L002531/1). Funding for the CCE was provided by The David and Lucile Packard Foundation, Natural Environment Research Council (Grant No. NE/K011480/1), U.S. Geological Survey (USGS) Sediment Transport in Coastal Environments Project, and Ocean University of China. MAC was supported by the UK National Capability NERC CLASS program (NERC Grant No. NE/R015953/1) and NERC Grants (NE/P009190/1, NE/P005780/1). MJBC is supported by a Royal Society Research Fellowship (DHF\R1\180166). PJT and DRP are supported by NE/S009965/1 and NE/R001952/1. We also thank David Piper, Chris Goldfinger and Editor Jean-Philippe Avouac for their insightful reviews, which subsequently improved the manuscript.

Appendix A. Supplementary material

Supplementary material related to this article can be found online at https://doi.org/10.1016/j.epsl.2021.116845.

References

Azpiroz-Zabala, M., Cartigny, M.J.B., Talling, P.J., Parsons, D.R., Sumner, E.J., Clare, M.A., Simmons, S.M., Cooper, C., Pope, E.L., 2017. Newly recognized turbidity current structure can explain prolonged flushing of submarine canyons. Sci. Adv. 3 (10), e1700200.

Bennett, R.H., Faris, J.R., 1979. Ambient and dynamic pore pressures in fine-grained submarine sediments: Mississippi Delta. Appl. Ocean Res. 1 (3), 115–123.

Bornhold, B.D., Ren, P., Prior, D.B., 1994. High-frequency turbidity currents in British Columbia fjords. Geo Mar. Lett. 14 (4), 238–243.

Canals, M., Puig, P., De Madron, X.D., Heussner, S., Palanques, A., Fabres, J., 2006. Flushing submarine canyons. Nature 444 (7117), 354–357.

Carter, L., Burnett, D., Drew, S., Hagadorn, L., Marle, G., Bartlett-McNeil, D., Irvine, N., 2009. Submarine Cables and the Oceans — Connecting the World. UNEP-WCMC Biodiversity Series, vol. 31. ICPC/UNEP/UNEP-WCMC (64 pp).

Carter, L., Milliman, J.D., Talling, P.J., Gavey, R., Wynn, R.B., 2012. Near-synchronous and delayed initiation of long run-out submarine sediment flows from a record-breaking river flood, offshore Taiwan. Geophys. Res. Lett. 39 (12), 6–10.

Casagrande, J., Watson, F., 2003. Hydrology and Water Quality of the Carmel and Salinas Lagoons, Monterey Bay, California: 2002/2003. Central Coast Watershed Studies Report No. WI-2003-14 to the Monterey County Water Resources Agency Board, 128 pp.

Chamberlain, T.K., 1964. Mass transport of sediment in the heads of Scripps Submarine Canyon, California. In: Papers in Marine Geology, Shepard Commemorative Volume. Macmillan Company, New York, pp. 42–64.

Christian, H.A., Woeller, D.J., Robertson, P.K., Courtney, R.C., 1997. Site investigations to evaluate flow liquefaction slides at Sand Heads, Fraser River delta. Can. Geotech. J. 34 (3), 384–397.

Clare, M.A., Hughes Clarke, J.E., Talling, P.J., Cartigny, M.J.B., Pratomo, D.G., 2016. Preconditioning and triggering of offshore slope failures and turbidity currents revealed by most detailed monitoring yet at a fjord-head delta. Earth Planet. Sci. Lett. 450, 208–220.

de Bettignies, F., Dauby, P., Thomas, F., Gobet, A., Delage, L., Bohner, O., Loisel, S., Davoult, D., 2020. Degradation dynamics and processes associated with the accumulation of Laminaria hyperborea (Phaeophyceae) kelp fragments: an in situ experimental approach. J. Phycol.

Dean, R.G., Dalrymple, R.A., 1991. Water Wave Mechanics for Engineers and Scientists (Vol. 2). World Scientific Publishing (353 pp).

Dugan, B., Sheahan, T.C., 2012. Offshore sediment overpressures of passive margins: mechanisms, measurement, and models. Rev. Geophys. 50 (3), 1–20.

Eittreim, S.L., Xu, J.P., Noble, M., Edwards, B.D., 2002. Towards a sediment budget for the Santa Cruz shelf. Mar. Geol. 181 (1–3), 235–248.

Farnsworth, K.L., Warrick, J.A., 2007. Sources, Dispersal, and Fate of Fine Sediment Supplied to Coastal California. U.S. Geological Survey, Reston, VA.

Fleckenstein, J.H., Niswonger, R.G., Fogg, G.E., 2006. River-aquifer interactions, geologic heterogeneity, and low-flow management. Groundwater 44 (6), 837–852.

Flemings, P.B., Long, H., Dugan, B., Germaine, J., John, C., Behrmann, J.H., Sawyer, D., 2008. Pore pressure penetrometers document high overpressure near the seafloor where multiple submarine landslides have occurred on the continental slope, offshore Louisiana, Gulf of Mexico. Earth Planet. Sci. Lett. 269 (3–4), 309–325.

Galy, V., France-Lanord, C., Beyssac, O., Faure, P., Kudrass, H., Palhol, F., 2007. Efficient organic carbon burial in the Bengal fan sustained by the Himalayan erosional system. Nature 450 (7168).

Gavey, R., Carter, L., Liu, J.T., Talling, P.J., Hsu, R., Pope, E., Evans, G., 2017. Frequent sediment density flows during 2006 to 2015, triggered by competing seismic and weather events: observations from subsea cable breaks off southern Taiwan. Mar. Geol. 384, 147–158.

Goldfinger, C., 2011. Submarine paleoseismology based on turbidite records. Annu. Rev. Mar. Sci. 3 (1), 35–66.

Gray, A.B., Pasternack, G.B., Watson, E.B., Warrick, J.A., Goñi, M.A., 2015. Effects of antecedent hydrologic conditions, time dependence, and climate cycles on the suspended sediment load of the Salinas River, California. J. Hydrol. 525, 632–649.

Greene, H., 1990. Regional Tectonics and Structural Evolution of the Monterey Bay Region, Central California.

Hage, S., Cartigny, M.J.B., Sumner, E.J., Clare, M.A., Hughes Clarke, J.E., Talling, P.J., Lintern, D.G., Simmons, S.M., Jacinto, R.S., Vellinga, A.J., Allin, J.R., Azpiroz-Zabala, M., Gales, J.A., Hizzett, J.L., Hunt, J.E., Mozzato, A., Parsons, D.R., Pope, E.L., Stacey, C.D., Symons, W.O., Vardy, M.E., Watts, C., 2019. Direct monitoring reveals initiation of turbidity currents from extremely dilute river plumes. Geophys. Res. Lett. 460, 11310–11320.

Harrold, C., Light, K., Lisin, S., 1998. Organic enrichment of submarine-canyon and continental-shelf benthic communities by macroalgal drift imported from nearshore kelp forests. Limnol. Oceanogr. 43 (4), 669–678.

Heerema, C.J., Talling, P.J., Cartigny, M.J., Paull, C.K., Bailey, L., Simmons, S.M., Parsons, D.R., Clare, M.A., Gwiazda, R., Lundsten, E., Anderson, K., Maier, K.L., Xu, J.P., Sumner, E.J., Rosenberger, K.J., Gales, J., McGann, M., Carter, L., Pope, E., the Monterey Coordinated Canyon Experiment (CCE) Team, 2020. What determines the downstream evolution of turbidity currents? Earth Planet. Sci. Lett. 532, 116023.

Heezen, B.C., Ewing, W.M., 1952. Turbidity currents and submarine slumps, and the 1929 Grand Banks earthquake. Am. J. Sci. 250 (12), 849–873.

Heezen, B.C., Ewing, M., Johnson, G.L., 1966. The Gulf of Corinth floor. Deep-Sea Res. Oceanogr. Abstr. 13 (3), 381–411.

Heezen, B.C., Menzies, R.J., Schneider, E.D., Ewing, W.M., Granelli, N.C.L., 1964. Congo submarine canyon. AAPG Bull. 48 (7), 1126–1149.

Hizzett, J.L., Hughes Clarke, J.E., Sumner, E.J., Cartigny, M.J.B., Talling, P.J., Clare, M.A., 2018. Which triggers produce the most erosive, frequent, and longest runout turbidity currents on deltas? Geophys. Res. Lett. 45 (2), 855–863.

Hsu, S.-K., Kuo, J., Lo, C.-L., Tsai, C.-H., Doo, W.-B., Ku, C.-Y., Sibuet, J.-C., 2008. Turbidity currents, submarine landslides and the 2006 Pingtung earthquake off SW Taiwan. Terr. Atmos. Ocean. Sci. 19 (6), 767.

Hughes Clarke, J.E., Marques, C.R.V., Pratomo, D., 2014. Imaging active mass-wasting and sediment flows on a fjord delta, Squamish, British Columbia. In: Submarine Mass Movements and Their Consequences. Springer, Cham, pp. 249–260.

Ikehara, K., Irino, T., Usami, K., Jenkins, R., Omura, A., Ashi, J., 2014. Possible submarine tsunami deposits on the outer shelf of Sendai Bay, Japan resulting from the 2011 earthquake and tsunami off the Pacific coast of Tohoku. Mar. Geol. 358, 120–127.

Inman, D.L., Nordstrom, C.E., Flick, R.E., 1976. Currents in submarine canyons: an air-sea-land interaction. Annu. Rev. Fluid Mech. 8 (1), 275–310.
Iverson, R.M., 2005. Debris-flow mechanics. In: Debris-Flow Hazards and Related Phenomena. Springer, Berlin, Heidelberg, pp. 105–134.
Johnson, K.S., Paull, C.K., Barry, J.P., Chavez, F.P., 2001. A decadal record of underflows from a coastal river into the deep sea. Geology 29 (11), 1019–1022.
Khripounoff, A., Vangriesheim, A., Crassous, P., Etoubleau, J., 2009. High frequency of sediment gravity flow events in the Var submarine canyon (Mediterranean Sea). Mar. Geol. 263 (1–4), 1–6.
Komar, P.D., Inman, D.L., 1970. Longshore sand transport on beaches. J. Geophys. Res. 75 (30), 5914–5927.
Liu, J.T., Wang, Y.H., Yang, R.J., Hsu, R.T., Kao, S.J., Lin, H.L., Kuo, F.H., 2012. Cyclone-induced hyperpycnal turbidity currents in a submarine canyon. J. Geophys. Res., Oceans 117 (4), 1–12.
Maier, K.L., Rosenberger, K.J., Paull, C.K., Gwiazda, R., Gales, J.A., Lorenson, T.D., Barry, J.P., Talling, P.J., McGann, M., Xu, J.P., Lundsten, E., Anderson, K., Litvin, S.Y., Parsons, D.R., Clare, M.A., Simmons, S.M., Sumner, E.S., Cartigny, M.J., 2019. Sediment and organic carbon transport and deposition driven by internal tides along Monterey Canyon, offshore California. Deep-Sea Res., Part I, Oceanogr. Res. Pap., 103108.
Major, J.J., Iverson, R.M., 1999. Debris-flow deposition: effects of pore-fluid pressure and friction concentrated at flow margins. Geol. Soc. Am. Bull. 111 (10), 1424–1434.
Martín, J., Palanques, A., Vitorino, J., Oliveira, A., de Stigter, H.C., 2011. Near-bottom particulate matter dynamics in the Nazaré submarine canyon under calm and stormy conditions. Deep-Sea Res., Part II, Top. Stud. Oceanogr. 58 (23–24), 2388–2400.
Masson, D.G., Wynn, R.B., Talling, P.J., 2010. Large landslides on passive continental margins: processes, hypotheses and outstanding questions. In: Submarine Mass Movements and Their Consequences, vol. 28, pp. 153–165.
Mastbergen, D.R., Van Den Berg, J.H., 2003. Breaching in fine sands and the generation of sustained turbidity currents in submarine canyons. Sedimentology 50 (4), 625–637.
Milliman, J.D., Meade, R.H., 1983. World-wide delivery of river sediment to the oceans. J. Geol. 91 (1), 1–21.
Mordecai, G., Tyler, P.A., Masson, D.G., Huvenne, V.A.I., 2011. Litter in submarine canyons off the west coast of Portugal. Deep-Sea Res., Part II, Top. Stud. Oceanogr. 58 (23–24), 2489–2496.
Mountjoy, J.J., Howarth, J.D., Orpin, A.R., Barnes, P.M., Bowden, D.A., Rowden, A.A., Schimel, A.C., Holden, C., Horgan, H.J., Nodder, S.D., Patton, J.R., Lamarche, G., Gerstenberger, M., Micallef, A., Pallentin, A., Kane, T., 2018. Earthquakes drive large-scale submarine canyon development and sediment supply to deep-ocean basins. Sci. Adv. 4 (3).
Mulder, T., Migeon, S., Savoye, B., Faugères, J.-C., 2001. Inversely graded turbidite sequences in the deep Mediterranean: a record of deposits from flood-generated turbidity currents? Geo Mar. Lett. 21 (2), 86–93.
Mulder, T., Syvitski, J.P.M., 1995. Turbidity currents generated at river mouths during exceptional discharges to the world oceans. J. Geol. 103 (3), 285–299.
Normandeau, A., Bourgault, D., Neumeier, U., Lajeunesse, P., St-Onge, G., Gostiaux, L., Chavanne, C., 2020. Storm-induced turbidity currents on a sediment-starved shelf: insight from direct monitoring and repeat seabed mapping of upslope migrating bedforms. Sedimentology 67 (2), 1045–1068.
Okey, T.A., 1997. Sediment flushing observations, earthquake slumping, and benthic community changes in Monterey Canyon head. Cont. Shelf Res. 17 (8), 877–897.
Özener, P.T., Özaydın, K., Berilgen, M.M., 2009. Investigation of liquefaction and pore water pressure development in layered sands. Bull. Earthq. Eng. 7 (1), 199–219.
Parsons, J.D., Bush, J.W.M., Syvitski, J.P.M., 2001. Hyperpycnal plume formation from riverine outflows with small sediment concentrations. Sedimentology 48 (2), 465–478.
Patsch, K., Griggs, G.B., 2006. Littoral Cells, Sand Budgets, and Beaches: Understanding California's Shoreline. Institute of Marine Sciences, University of California, Santa Cruz (40 pp).
Paull, C.K., Ussler III, W., Greene, H.G., Keaten, R., Mitts, P., Barry, J., 2003. Caught in the act: the 20 December 2001 gravity flow event in Monterey Canyon. Geo Mar. Lett. 22 (4), 227–232.
Paull, C.K., Mitts, P., Ussler III, W., Keaten, R., Greene, H.G., 2005. Trail of sand in upper Monterey Canyon: offshore California. Bull. Geol. Soc. Am. 117 (41921), 1134.
Paull, C.K., Ussler III, W., Caress, D.W., Lundsten, E., Covault, J.A., Maier, K.L., Xu, J., Augenstein, S., 2010. Origins of large crescent-shaped bedforms within the axial channel of Monterey Canyon, offshore California. Geosphere 6 (6), 755–774.
Paull, C.K., Caress, D.W., Lundsten, E., Gwiazda, R., Anderson, K., McGann, M., Conrad, J., Edwards, B., Sumner, E.J., 2013. Anatomy of the La Jolla Submarine Canyon system; offshore southern California. Mar. Geol. 335, 16–34.
Paull, C.K., Talling, P.J., Maier, K.L., Parsons, D., Xu, J., Caress, D.W., Gwiazda, R., Lundsten, E.M., Anderson, K., Barry, J.P., Chaffey, M., O'Reilly, T., Rosenberger, K.J., Gales, J.A., Kieft, B., McGann, M., Simmons, S.M., McCann, M., Sumner, E.J., Clare, M.A., Cartigny, M.J., 2018. Powerful turbidity currents driven by dense basal layers. Nat. Commun. 9 (1), 1–9.
Piper, D.J.W., Cochonat, P., Morrison, M.L., 1999. The sequence of events around the epicentre of the 1929 Grand Banks earthquake: initiation of debris flows and turbidity current inferred from sidescan sonar. Sedimentology 46 (1), 79–97.
Piper, D.J.W., Savoye, B., 1993. Processes of Late Quaternary turbidity-current flow and deposition on the Var deep-sea fan, north-west Mediterranean Sea. Sedimentology 40, 557–582.
Pope, E.L., Talling, P.J., Carter, L., Clare, M.A., Hunt, J.E., 2017. Damaging sediment density flows triggered by tropical cyclones. Earth Planet. Sci. Lett. 458, 161–169.
Puig, P., Ogston, A.S., Mullenbach, B.L., Nittrouer, C.A., Parsons, J.D., Sternberg, R.W., 2004. Storm-induced sediment gravity flows at the head of the Eel submarine canyon, northern California margin. J. Geophys. Res., Oceans 109 (C3), 1–10.
Puig, P., Canals, M., Company, J.B., Martín, J., Amblas, D., Lastras, G., Palanques, A., Calafat, A.M., 2012. Ploughing the deep sea floor. Nature 489 (7415), 286–289.
Puig, P., Greenan, B.J.W., Li, M.Z., Prescott, R.H., Piper, D.J.W., 2013. Sediment transport processes at the head of Halibut Canyon, eastern Canada margin: an interplay between internal tides and dense shelf-water cascading. Mar. Geol. 341, 14–28.
Rao, J.S., Liu, H., 2017. Discordancy partitioning for validating potentially inconsistent pharmacogenomic studies. Sci. Rep. 7 (1), 15169.
Rosenberger, K.J., Storlazzi, C.D., Cheriton, O.M., 2016. Variability of the internal tide on the southern Monterey Bay continental shelf and associated bottom boundary layer sediment transport. Cont. Shelf Res. 120, 68–81.
Simmons, S.M., Azpiroz-Zabala, M., Cartigny, M.J.B., Clare, M.A., Cooper, C., Parsons, D.R., Pope, E.L., Sumner, E.J., Talling, P.J., 2020. Novel acoustic method provides first detailed measurements of sediment concentration structure within submarine turbidity currents. J. Geophys. Res., Oceans.
Smith, D.P., Kvitek, R., Iampietro, P.J., Wong, K., 2007. Twenty-nine months of geomorphic change in upper Monterey Canyon (2002-2005). Mar. Geol. 236 (1–2), 79–94.
Smith, D.P., Ruiz, G., Kvitek, R., Iampietro, P.J., 2005. Semiannual patterns of erosion and deposition in upper Monterey Canyon from serial multibeam bathymetry. Bull. Geol. Soc. Am. 117 (9–10), 1123–1133.
Stegmann, S., Sultan, N., Kopf, A., Apprioual, R., Pelleau, P., 2011. Hydrogeology and its effect on slope stability along the coastal aquifer of Nice, France. Mar. Geol. 280 (1–4), 168–181.
Stevens, T., Paull, C.K., Ussler III, W., McGann, M., Buylaert, J.-P., Lundsten, E., 2014. The timing of sediment transport down Monterey Submarine Canyon, offshore California. GSA Bull. 126 (1–2), 103–121.
Talling, P.J., 2014. On the triggers, resulting flow types and frequencies of subaqueous sediment density flows in different settings. Mar. Geol. 352, 155–182.
Talling, P., Clare, M., Urlaub, M., Pope, E., Hunt, J., Watt, S., 2014. Large submarine landslides on continental slopes: geohazards, methane release, and climate change. Oceanography 27 (2), 32–45.
Thornton, E.B., 2016. Temporal and spatial variations in sand budgets with application to southern Monterey Bay, California. Mar. Geol. 382, 56–67.
Van Den Berg, J.H., Van Gelder, A., Mastbergen, D.R., 2002. The importance of breaching as a mechanism of subaqueous slope failure in fine sand. Sedimentology 49 (1), 81–95.
Vendettuoli, D., Clare, M.A., Hughes Clarke, J.E., Vellinga, A., Hizzet, J., Hage, S., Cartigny, M.J.B., Talling, P.J., Waltham, D., Hubbard, S.M., Stacey, C., Lintern, D.G., 2019. Daily bathymetric surveys document how stratigraphy is built and its extreme incompleteness in submarine channels. Earth Planet. Sci. Lett. 515, 231–247.
Watson, F., Anderson, T., Casagrande, J., Kozlowski, D., Newman, W., Hager, J., Smith, D.P., Curry, R., 2003. Salinas Valley Sediment Sources. Central Coast Watershed Studies Report No. WI-2002-10 to the California Central Coast Water Quality Control Board, pp. 239.
Willis, C.M., Griggs, G.B., 2003. Reductions in fluvial sediment discharge by coastal dams in California and implications for beach sustainability. J. Geol. 111 (2), 167–182.
Xu, J.P., Noble, M.A., Rosenfeld, L.K., 2004. In-situ measurements of velocity structure within turbidity currents. Geophys. Res. Lett. 31 (9).
Xu, J.P., Swarzenski, P.W., Noble, M., Li, A.C., 2010. Event-driven sediment flux in Hueneme and Mugu submarine canyons, southern California. Mar. Geol. 269 (1–2), 74–88.
Zhang, Y., Liu, Z., Zhao, Y., Colin, C., Zhang, X., Wang, M., Zhao, S., Kneller, B., 2018. Long-term in situ observations on typhoon-triggered turbidity currents in the deep sea. Geology 46 (8), 675–678.